ADVANCED MATERIALS
www.advmat.de

Indoor Photovoltaic Fiber with an Efficiency of 25.53% under 1500 Lux Illumination

*Zhengfeng Zhu, Zhengmeng Lin, Weijie Zhai, Xinyue Kang, Jiatian Song, Chenhao Lu, Hongyu Jiang, Peining Chen, Xuemei Sun, Bingjie Wang, Zhong-Sheng Wang, and Huisheng Peng**

Photovoltaic devices represent an efficient electricity generation mode. Integrating them into textiles offers exciting opportunities for smart electronic textiles—with the ultimate goal of supplying power for wearable technology—which is poised to change how electronic devices are designed. Many human activities occur indoors, so realizing indoor photovoltaic fibers (IPVFs) that can be woven into textiles to power wearables is critical, although currently unavailable. Here, a dye-sensitized IPVF is constructed by incorporating titanium dioxide nanoparticles into aligned nanotubes to produce close contact and stable interfaces among active layers on a curved fiber substrate, thus presenting efficient charge transport and low charge recombination in the photoanode. With the combination of highly conductive core–sheath Ti/carbon nanotube fiber as a counter electrode, the IPVF shows a certified power conversion efficiency of 25.53% under 1500 lux illuminance. Its performance variation is below 5% after bending, twisting, or pressing for 1000 cycles. These IPVFs are further integrated with fiber batteries as self-charging power textiles, which are demonstrated to effectively supply electricity for wearables, solving the power supply problem in this important direction.

1. Introduction

Wearable electronic devices are booming for many important application fields,[1–5] such as communication, global positioning, healthcare, sensing, and interaction, thus posing an ever-growing demand for flexible, lightweight, and especially sustainable power supplies.[6–9] People staying someplace with available electricity all the time is impractical because of their complex and uncertain activities, including working, playing, moving, staying, and exercising. Hence, extra energy harvesting to replenish electricity at any time is of particular importance for current wearables, particularly emerging electronic textiles. Similar to sunlight for solar cells,[10–12] indoor light is a widely available energy to be exploited for photovoltaic devices,[13–18] but it has been almost wasted. As estimated, global lighting consumes far beyond a trillion kilowatt-hours (kWh) every year, even accounting for ≈20% of the total electricity consumption in the world.[19] Reusing wasted indoor light energy is worthwhile, but directly setting photovoltaic panels that occupy a vast space in a room seems rather impracticable. Inspiringly, many human activities occur indoors, and the bodies of humans provide suitable platforms for indoor photovoltaic devices. Therefore, making indoor photovoltaic fibers (IPVFs) and then weaving them into textiles offers exciting opportunities for indoor power solutions, hopefully generating electricity to effectively power wearable electronic products. Moreover, if IPVFs are integrated with fiber batteries to support displays, sensors, and microchips also in fiber shape to produce smart electronic textiles,[20–23] then they may pave the way to next-generation personal health management and emergency alerts (**Figure 1**a–c). Despite the urgent demand for IPVFs, synthesizing appropriate materials and constructing matchable microstructures with compact interfaces on curved fibers for efficient charge separation and transport is difficult, and the severe interfacial charge recombination produced induces performance deterioration; this issue could be more serious under dim indoor light than under sunlight,[14,24–26] making efficient IPVFs as yet unavailable.

Dye-sensitized photovoltaic devices with advantages of easy preparation, low cost, high performance even in fiber type, and especially high response to dim light exhibit wide prospects in indoor applications,[27] while the difficulty in developing fiber electrodes has seriously restricted the realization of efficient dye-sensitized IPVFs. Here, we design an IPVF with a photoanode made from a radially aligned TiO_2 nanotube array incorporated

Z. Zhu, Z. Lin, W. Zhai, X. Kang, J. Song, C. Lu, H. Jiang, P. Chen, X. Sun, B. Wang, H. Peng
State Key Laboratory of Molecular Engineering of Polymers
Department of Macromolecular Science and Laboratory of Advanced Materials
Fudan University
Shanghai 200438, China
E-mail: penghs@fudan.edu.cn
Z.-S. Wang
Department of Chemistry
Fudan University
Shanghai 200438, China

The ORCID identification number(s) for the author(s) of this article can be found under https://doi.org/10.1002/adma.202304876

DOI: 10.1002/adma.202304876

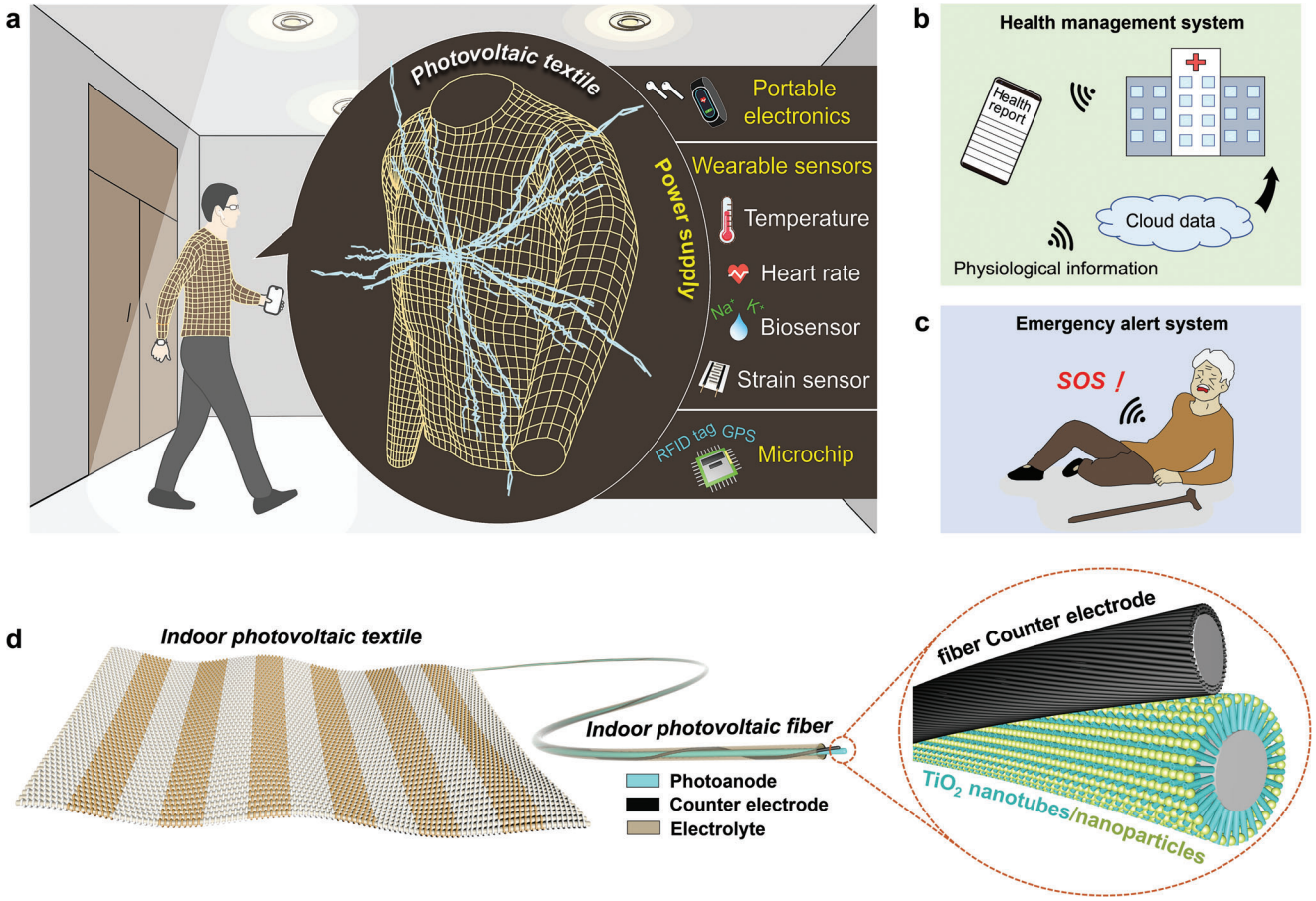

Figure 1. Schematic diagrams of the IPVF. a) Schematic showing an indoor power solution exploiting indoor light to generate electricity by photovoltaic textiles to power various wearable electronics, such as portable electronic products, miniaturized biosensors, motion sensors, and multifunctional microchips. b,c) Schematics showing power supply textiles integrated with other functional components to innovate the architectures and functions of wearables, such as wearable smart textiles with health management systems (b) and emergency alert systems (c), to protect the health and life safety of human beings. d) Indoor photovoltaic textile made from IPVFs with a photoanode (TiO_2 nanotube array incorporated with nanoparticles), a counter electrode (CNT sheet closely attached on a metal fiber), an electrolyte, and an encapsulated tube.

with TiO_2 nanoparticles on a Ti wire and a counter electrode composed of an axially aligned carbon nanotube (CNT) sheet closely attached to another Ti wire (Figure 1d). In the hybrid TiO_2 layer, the TiO_2 nanoparticle film that fully covered the nanotube array ensured sufficient dye loading in the photoanode, and their seamless and stable interfaces realized rapid charge transport through the TiO_2 nanotubes and lower charge recombination. The design of an aligned CNT sheet as the sheath and a Ti wire as the core dramatically enhanced the electrical conductivity of the counter electrode to promote interfacial charge collection and transport. The IPVF showed a high certified power conversion efficiency (PCE) of 25.53% under 1500 lux illumination, with both high flexibility and stability.

2. Results and Discussion

The IPVF can be produced as schematically illustrated in **Figure** 2a. Briefly, after anodization and dip-coating with a TiO_2 nanoparticle slurry, a Ti wire was annealed and sensitized to act as the photoanode. The aligned CNT sheet synthesized by chemical vapor deposition was wound on another Ti wire and then twisted around the photoanode wire as the counter electrode. Finally, the photoanode and counter electrode were encapsulated in a transparent tube, followed by the injection of an electrolyte to produce the IPVF (Figure S1, Supporting Information, Figure 2b).

The lengths of the TiO_2 nanotubes were easily adjusted by changing the anodization time (Figure S2, Supporting Information). However, "V-type" gaps inevitably emerged among TiO_2 nanotubes according to their geometric distribution and became more serious with increasing length. Low specific surface areas and volume losses of nanotubes would seriously restrict dye loading in the photoanode. Hence, we designed a strategy of incorporating TiO_2 nanoparticles among TiO_2 nanotubes to construct a hybrid TiO_2 layer by the dip-coating method (Figure 2c,d). High dispersion and viscosity of the TiO_2 nanoparticle slurry were critical to making the desired uniform nanoparticle layer on an irregular surface. As a typical nanofluid, the viscosity of the TiO_2 slurry is strongly related to the volume fraction of nanoparticles.[28–30] After we sharply increased the content of TiO_2 nanoparticles highly dispersed in the slurry to 25 wt%, its viscosity was effectively enhanced to reduce the impact of surface tension so

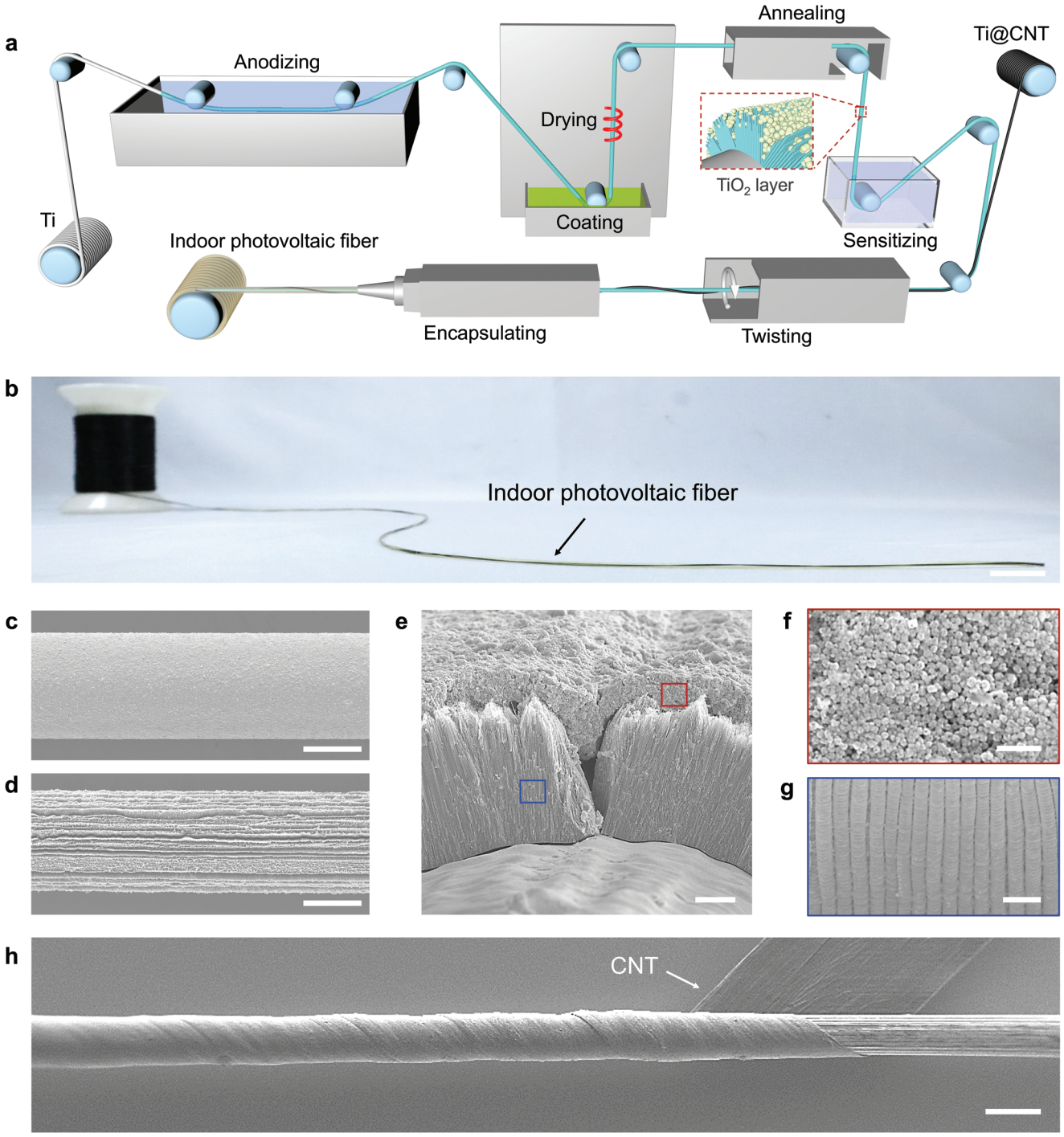

Figure 2. Preparation and structure of the IPVF. a) Sketch map depicting the flow of the IPVF fabrication process. The photoanode was prepared from Ti wire by anodization, dip-coating, annealing, and sensitization in sequence. The CNT-based counter electrode was twisted around the photoanode and encapsulated in a transparent tube. b) Photograph of a roll of IPVFs. c,d) SEM images of TiO_2 nanotube arrays with (c) and without (d) incorporated TiO_2 nanoparticles. The hybrid TiO_2 layer show a uniform and smooth surface, indicating the high quality of the TiO_2 nanoparticle film. e) Cross-sectional SEM image of the TiO_2 layer, where incorporated TiO_2 nanoparticles filled in the gaps of the TiO_2 nanotube array to produce a compact interface between them. f,g) High-resolution SEM images of TiO_2 nanoparticles (f) and the TiO_2 nanotube array (g) marked in (e). The nanoparticles display uniform sizes of ≈30 nm, and their high specific areas were beneficial for sufficiently adsorbing sensitizers. The aligned TiO_2 nanotubes show an average diameter of 170 nm, which can provide rapid transport channels for generated charges. h) SEM image of the counter electrode. The aligned CNT sheet was closely attached to a Ti wire to form a core–sheath structure. Scale bars: 2 cm in (b), 100 µm in (c) and (d), 5 µm in (e), 200 nm in (f), 500 nm in (g), and 50 µm in (h).

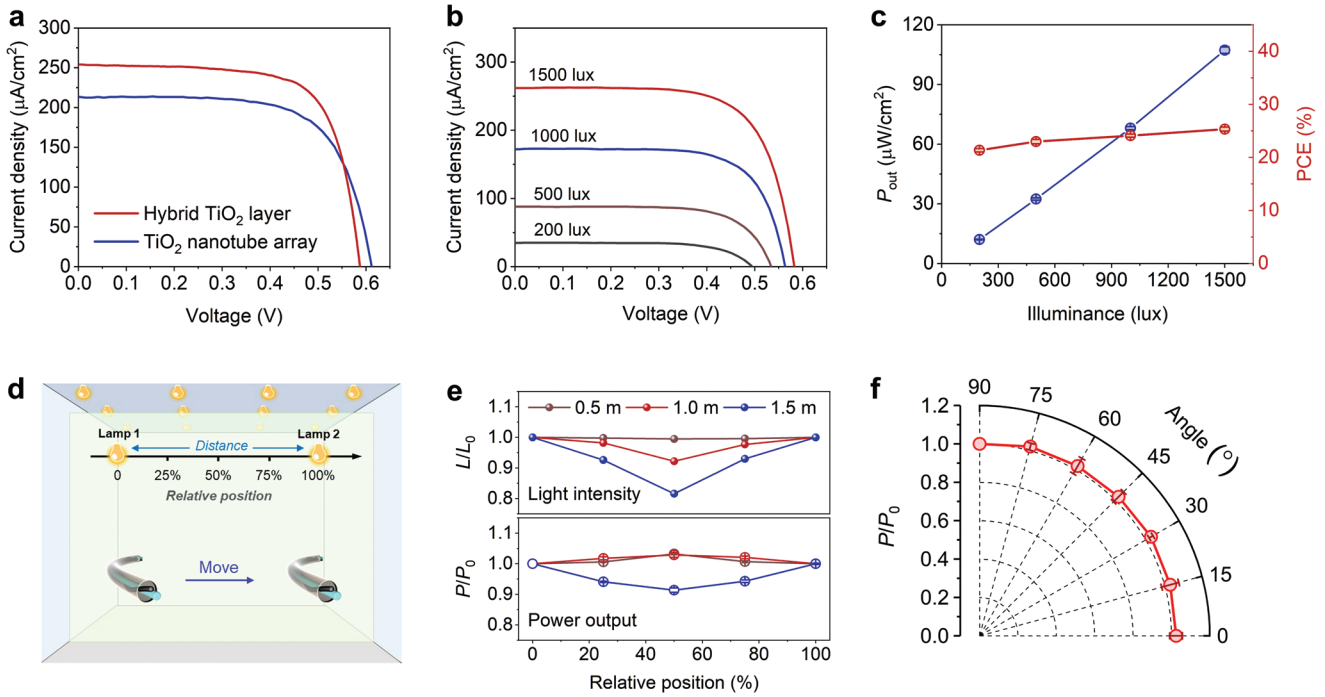

Figure 3. Photovoltaic properties of IPVFs. a) *J–V* curves of IPVFs with and without incorporation of TiO_2 nanoparticles measured under 1500 lux illuminance. The IPVF with the hybrid TiO_2 layer showed a J_{SC} of 254.05 μA cm^{-2}, a V_{OC} of 0.5874 V, and an *FF* of 72.44%, producing a PCE of 25.53%. Active area, 0.0185 cm^2. The IPVF with the bare TiO_2 nanotube array showed a J_{SC} of 212.79 μA cm^{-2}, a V_{OC} of 0.611 V, and an *FF* of 67.98%, presenting a PCE of 20.88%. Active area, 0.0177 cm^2. The incorporated nanoparticles dramatically improved the sensitizer adsorption and interfaces to enhance both the photocurrent and *FF*. b) *J–V* curves of IPVFs measured under different indoor illuminance intensities. Active area, 0.0185 cm^2. The IPVFs can steadily work under illumination intensities from 200 to 1500 lux, which mimic various indoor scenes. c) Power outputs and PCEs of IPVFs under different indoor illuminances. Error bars: standard deviations of the results from three samples. d) Diagram illustrating the distribution of indoor lamps and the position of the IPVF under them. Two lamps were designed as objects, and an IPVF was located under them and moved from one side to the other. The integrated light intensity vertical on the IPVF was influenced by the distance from the lamps and the relative position of the IPVF. e) Incident light intensities in the vertical direction and corresponding power output of IPVFs at different positions under lamps. Error bars, standard deviations of the results from three samples. When the distance between lamps was 1.5 m, the lowest intensity of vertically incident light was 81.6%, while the PCE of the IPVF was maintained at 91.4% due to the additional light absorption by the sides. f) Power output of the IPVF under incident light from different directions. Error bars, standard deviations of the results from three samples. When the lamp was directly above the IPVF, the corresponding angle was defined as 90°. For real applications, the angle would not exceed 90°.

that the slurry covering the irregular nanotube array produced a uniform nanoparticle layer without discontinuities, agglomerations or cracks (Figures S3 and S4, Supporting Information). The tightly incorporated hybrid TiO_2 layer with stronger mechanical properties would also resist more external pressures and frictions. In the hybrid TiO_2 layer, nanoparticles filled in the "V-type" gaps and formed compact interfaces with neighboring nanotubes (Figure 2e). Their large specific surface areas ensured efficient sensitizer adsorption (Figure 2f), while radially aligned TiO_2 nanotubes provided direct channels for rapid charge transport (Figure 2g).

We also designed a highly conducting counter electrode with a unique core-sheath structure, as both high catalytic activity and electrical conductivity are critical for the counter electrode[31] (Figure 2h; Figure S5a, Supporting Information). The aligned CNT sheet with high catalytic activity was continuously prepared by floating catalyst chemical vapor deposition (Figure S5b,c, Supporting Information), and it was then tightly wrapped around a Ti wire to achieve rapid charge collection and transport due to the radial hopping transport mechanism among CNTs[32] combined with the axial metal transport channels. Low-cost Ti wire with high chemical stability was used as a metal current collector to avoid its reaction with iodine in the electrolyte. The core–sheath counter electrode demonstrated both much lower electrical resistances and electrochemical impedances compared with the twisted bare CNT fiber typically investigated before, reflecting more rapid charge transport and ion diffusion (Figure S6, Supporting Information).

Here, a commercial N719 dye was chosen as the sensitizer because its absorption range precisely covers the light spectrum from a common fluorescent lamp, and I^-/I_3^- redox mediators with an optimal concentration were used in the electrolyte system for high transmittance (Figure S7, Supporting Information). Then, under 1500 lux illuminance, we first explored TiO_2 nanotube arrays as photoanodes in IPVFs by constructing a measurement system for accurate characterization (Figure S8, Supporting Information). When the thickness of the array was ≈19 μm, the IPVF achieved a PCE of 20.88%, with J_{SC}, V_{OC}, and *FF* of 212.79 μA cm^{-2}, 0.611 V, and 67.98%, respectively (**Figure 3a**). A further increase in the nanotube length did not effectively enhance the current density or PCE (Figure S9a, Table S1, Supporting Information). That is, their upper limits

had been reached, which were strongly restricted by the dye loading.

Although TiO_2 nanoparticles with large specific surface areas are widely used in planar devices, the dense nanoparticle layer formed due to the difficulty in constructing a porous structure on the fiber restrained efficient infiltration of the electrolyte, and their surface defect states could also trap more electrons to aggravate charge recombination;[33,34] thus, the resulting IPVF showed a lower PCE of 19.72%, with J_{SC}, V_{OC}, and *FF* of 214.57 μA cm^{-2}, 0.547 V, and 71.15%, respectively (Figure S9b, Supporting Information). According to the dependence of V_{OC} on the irradiation intensity, the ideality factor n ($1 < n < 2$) was calculated to evaluate the trap-assisted nonideal recombination in the IPVF[27] (Methods). The high n value of 1.72 demonstrated serious nonradiative charge carrier recombination in the IPVF, which could induce a large voltage loss, especially under dim light[24,35–37] (Figure S9c, Supporting Information).

The photovoltaic performance of the IPVF was very limited from either the TiO_2 nanotube array or nanoparticle layer, but their intimate incorporation represented a promising strategy for achieving both sufficient light harvesting and low charge recombination. After we successfully constructed the hybrid TiO_2 layer in IPVFs, sufficient light harvesting generated a higher photocurrent, and the stable interfaces promoted efficient charge transport through nanotubes for lower charge recombination, which was consistent with the low ideality factor of 1.28, thus achieving higher J_{SC}, V_{OC} and *FF* to produce a PCE over 25% (Figure S9c–e, Table S2, Supporting Information). The TiO_2 nanoparticles showed optimal thicknesses of 3–5 μm for the best photovoltaic performance. A too-thin film was insufficient for loading adequate sensitizers, while a too-thick nanoparticle layer would induce more trap-assisted nonideal recombination, causing performance degradation. Moreover, PCEs with a narrow distribution from 30 IPVFs measured under 1500 lux illuminance demonstrated both high repeatability and stability of this fabrication method (Figure S9f, Supporting Information).

We further characterized the charge transport properties in IPVFs with different photoanodes by electrochemical impedance spectroscopy[38,39] (Experimental Section, Figure S10a–c, Table S3, Supporting Information), and the higher charge transfer resistance intuitively reflected the less charge recombination at the TiO_2/electrolyte interface, indicating the rapid charge transport through aligned TiO_2 nanotubes in the photoanode. Due to the direct charge transport channels provided by aligned TiO_2 nanotubes in the hybrid layer, the corresponding IPVF exhibited a much higher charge collection efficiency (η_{CC} = 99.36%), a lower electron transit time (τ_D = 12.38 ms), and a larger electron diffusion coefficient ($D_n = 4.27 \times 10^{-4}$ cm^2 s^{-1}) than those of the IPVF using the TiO_2 nanoparticle layer as the photoanode, demonstrating rapid charge transport and low charge recombination. Moreover, a continuous reading of electron lifetime (τ_n) as a function of photovoltage in IPVF using a simple open-circuit voltage decay technique also revealed significantly lower charge recombination in hybrid TiO_2 layer compared to TiO_2 nanoparticle layer[40] (Figure S10d,e, Supporting Information).

Finally, the IPVF achieved a high PCE of 25.53% under independent certification, with J_{SC}, V_{OC}, and *FF* as high as 254.05 μA cm^{-2}, 0.5874 V and 72.44%, respectively; a maximal power density of 108.11 μW cm^{-2} was realized (Figure 3a; Figure S11, Supporting Information). We also explored the counter electrode further loaded with Pt nanoparticles for IPVFs and obtained similar photovoltaic performance to the IPVF without Pt nanoparticles (Figure S12a, Supporting Information), indicating that the Ti/CNT fiber had achieved high enough electrical conductivity and catalytic property to satisfy IPVFs. Besides our designed fiber electrodes, the unique fiber shape of IPVFs also had contributions to their high PCEs, reflected in the enhanced photocurrents.[12,41] According to the geometrical structure, the cylindrical transparent tube and the electrolyte covered on the photoanode are similar to an optical lens, through which the incident light would be refracted. More incident light would be gathered on two sides of the photoanode, and effectively utilized by the fiber-shaped photoanode that could absorb the lateral light. Hence, fiber dye-sensitized photovoltaic devices could harvest more incident light to produce higher photocurrent, showing higher J_{SC} values.

These IPVFs could work over a wide range of 200–1500 lux illuminances mimicking indoor conditions to satisfy more real applications, despite suffering from slightly more voltage losses under weaker irradiation (Figure 3b,c, Table S4, Supporting Information). Due to the inherent device mechanism, the photovoltaic performance of IPVF under various ambient light intensities was similar to that of N719-dye and iodine electrolytes-based lab-scale cells, even though changing the device shape and area of IPVF. Certainly, the resulting IPVF could also efficiently work under sunlight in the case that it is also required for power supply outdoors, showing a high PCE of 10.11% under simulated AM 1.5G sunlight (Figure S12b, Supporting Information). Furthermore, IPVFs may be typically used under mobile conditions in the future; thus, the arrangement of lamps and relative locations of IPVFs are critical for the power output (Figure 3d). The integrated light intensity from two lamps generally shows the lowest value in the middle position between them, which may have a serious influence on IPVFs. Although the vertical light intensity was reduced to 81.6%, owing to the merit of the fiber shape in absorbing light from 360° directions, the IPVF could also exploit incident light from the lateral side to maintain the power output at 91.4% of the initial value, which is acceptable for real applications (Figure 3e,f).

Owing to the high reproducibility and low-cost preparation of our IPVFs (Table S5, Supporting Information), they could be further woven into textiles at a large scale and integrated with fiber batteries as self-charging power systems (**Figure 4a**). The output voltages and currents of photovoltaic modules in the power system could be controlled by connecting IPVFs in series or in parallel (Figure S13, Supporting Information). After the indoor light energy was harvested by IPVFs, they generated electricity that would charge fiber batteries and realize the electricity storage (Figure 4b). A fiber lithium-ion battery was successfully charged from 3 to 4 V under indoor light (Figure 4c,d; Figure S14, Supporting Information), showing an overall energy conversion and storage efficiency of 18.59% (Experimental Section, Supporting Information). The integrated power textiles demonstrated high mechanical stabilities against bending, twisting, and pressing, and the PCEs were maintained at over 95% after 1000 cycles (Figure 4e–g). The IPVFs could steadily work at increasing temperatures of −10 to 40 °C to

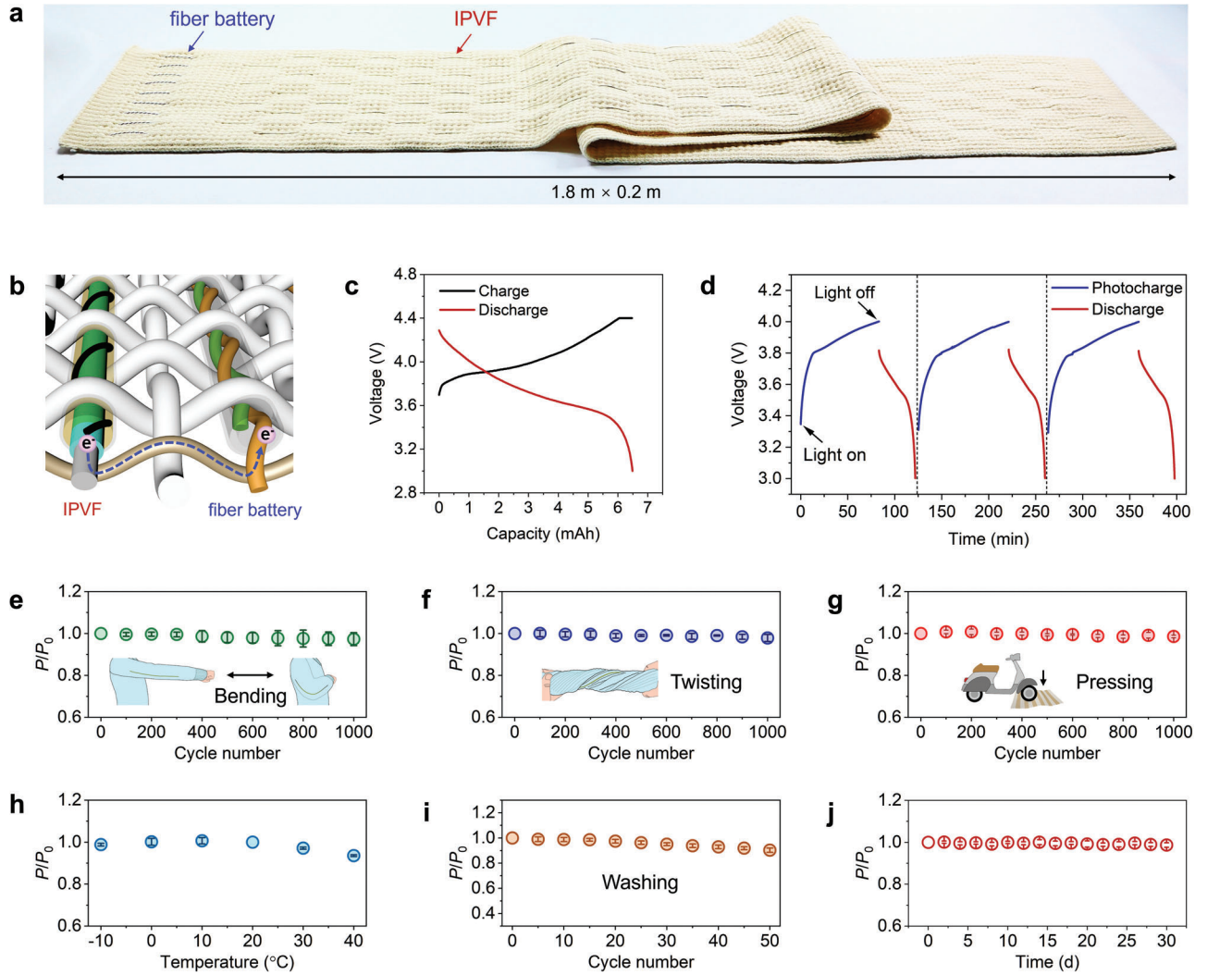

Figure 4. Properties of self-charging power textiles. a) Photograph of a self-powered textile with a size of 1.8 m × 0.2 m integrated with IPVFs and fiber batteries. b) Diagram illustrating the working mechanism of self-charging power textiles. After the IPVFs were connected in series and parallel for the designed output voltage and current, their lead wires from the photoanode and counter electrode were connected with the negative and positive electrodes from fiber batteries, respectively. Under indoor illumination, light energy was harvested and converted to electricity by IPVFs, which further charged fiber batteries to realize the storage of electricity. c) Typical charge and discharge profiles of a fiber lithium-ion battery. The fiber lithium-ion battery was first charged at 0.3 C from 3 to 4.4 V, then charged under 4.4 V until the current was below 0.05 C and subsequently discharged to 3 V at 0.5 C. d) Photocharge/discharge curves of the self-powered textile. The fiber lithium-ion battery was charged by the IPVF under 1500 lux illuminance from 3 to 4 V and then discharged to 3 V. e–g) Mechanical stability of the photovoltaic textile against bending (e), twisting (f), and pressing (g). Error bars: standard deviations of the results from three samples. The PCE was maintained at over 95% after 1000 cycles for each deformation mode. h) Stability of photovoltaic textiles at temperatures of −10 to 40 °C, showing PCE variations of less than 10%. Error bars: standard deviations of the results from three samples. i) Stability of photovoltaic textiles after washing for 15 min. Error bars, standard deviations of the results from three samples. The PCE variation was below 10% after the textiles were washed for 50 cycles. j) Long-term stability of photovoltaic textiles in air. Error bars, standard deviations of the results from three samples. Their performance varied by less than 5% after the textiles had been exposed to the air for 1 month.

satisfy different environments (Figure 4h), and also showed high stability under continuous irradiation from a general indoor light without obvious degradation (Figure S15, Supporting Information). Moreover, after they were washed with water for 50 cycles or placed in air for a month, their performance variations were less than 10% and 5%, respectively (Figure 4i,j; Figure S16, Supporting Information). The high stability of IPVF under 1500 lux illuminance may sufficiently represent their stability levels under various indoor illuminations, as the typically used weaker indoor irradiations would have less influence on IPVFs.

Our self-charging power textiles can also be designed in different sizes and styles to meet the energy demands of a variety of electronic devices (**Figure 5a**). A piece of clothing integrated with 0.2 m^2 IPVFs could theoretically output over 200 mW under 1500 lux illuminance, which can support the electricity required for most wearables. Hence, an exciting indoor power solution has been explored for portable electronics, health monitoring devices, and smart textiles.

These power textiles offer an effective solution to supply extra electricity for a variety of electronic systems (Figure 5b–f).

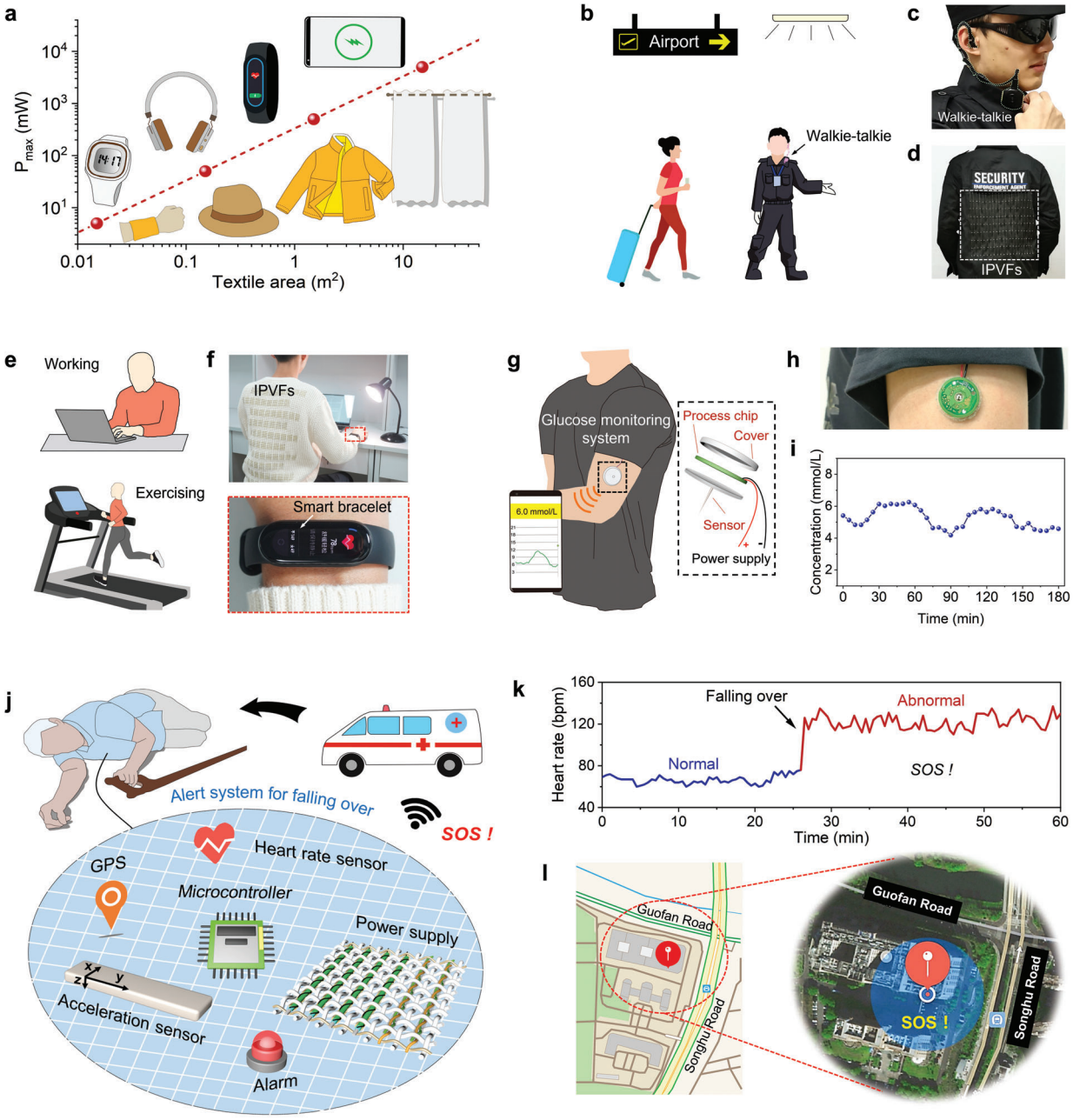

Figure 5. Wearable applications of self-charging power textiles. a) Power outputs of different textiles, in which the effective area of IPVFs accounted for 30%. Portable electronic products corresponding to the power outputs of self-charging power textiles are illustrated. b) Schematic plot illustrating self-charging power textiles to provide electricity for portable communication devices, such as wearable walkie-talkies equipped on workers in airports, who generally have to move to preserve order in public and provide help for people. Communication devices are widely used by these workers to keep in contact at work. These devices require a persistent operation, but there are few chances to replenish the electricity while working. c,d) Photographs displaying the textile to supply power for a walkie-talkie. Here, these self-charging power textiles present an effective solution to supply them with power. e) Schematic showing the self-powered textile to support electricity for a smart bracelet that can monitor the motions and heart rates in the daily work and exercise of human beings. f) Photograph of the IPVF textile integrated into clothing to supply power for a smart bracelet. g) Diagrammatic drawings of a wearable long-term glucose monitoring system integrated with the self-powered textile as a power source. The glucose information was continuously collected through the biosensor and transformed into visual data by the chip, which could be read from the terminal display. h) Photograph of the glucose monitoring system equipped on an arm. i) Real-time glucose concentrations obtained from the glucose monitoring system. j) Schematic illustrating a smart textile with an emergency alert system for falling over. The self-powered textile was used as a central energy module to integrate other functional components, including microcontrollers, a global positioning system, and sensors, to construct a smart textile. After the user fell over, the sensors detected abnormal signals of motion and heart rate, which were analyzed to determine whether the user was in danger. Once confirmed, the alert system rapidly transmitted messages for help and shared the real-time location. k) Real-time heart rate reflecting the normal or abnormal physiological status of the user after falling over. l) Emergency alert system sending messages for help and sharing the location on the map.

Particularly, they showed the effective application to powering a wearable long-term glucose monitoring system for healthcare, as a persistent power supply is crucial for long-term monitoring devices for specific people to monitor disease states and prevent serious illness (Figure 5g–i). Our self-charging power textiles may also be used as central energy modules to integrate various functional components, which may innovate the architectures and functions of wearable devices, for example, smart electronic textiles needed for our intelligent life. A conceptual wearable alert system against falling was illustrated by integrating self-charging power textiles with sensors, a global positioning system, and microchips (Figure 5j). After the user fell over, abnormal signals for motion and heart rate were detected by the sensors and analyzed to determine whether the user was in danger (Figure 5k). Once confirmed, the alert system immediately transmitted messages for help and further shared the real-time location (Figure 5l). The human experiments conformed to the regulation of the Animal and Human Experimentation Committee of Fudan University. A healthy subject from Fudan University had provided written, informed consent before participating in the study.

3. Conclusion

We have constructed an IPVF to obtain a certified PCE of 25.53% under 1500 lux illuminance. The IPVF can be integrated with fiber batteries into textiles as new self-charging power systems. If all people in the world wear such new power textiles and stay under indoor illuminance for 8 h every day, then the total generated electricity would reach over 5 billion kWh per year. These IPVFs may revolutionize portable, flexible, and wearable electronic technologies in the future.

Supporting Information

Supporting Information is available from the Wiley Online Library or from the author.

Acknowledgements

Z.Z., Z.L., and W.Z. contributed equally to this work. The authors thank Fusheng Li of the Department of Light Sources and Illuminating Engineering of Fudan University for assistance in the measurement of the fluorescent lamp. This work was supported by NSFC (52122310, 22075050, 52222310, T2222005, 22175042), STCSM (21511104900, 20JC1414902), and China Postdoctoral Science Foundation (2021M690659).

Conflict of Interest

The authors declare no conflict of interest.

Data Availability Statement

The data that support the findings of this study are available from the corresponding author upon reasonable request.

Keywords

fiber dye-sensitized solar cells, functional textiles, hybrid nano TiO_2, indoor photovoltaics, self-charging power systems

Received: May 23, 2023
Revised: August 3, 2023
Published online: December 24, 2023

[1] A. Libanori, G. Chen, X. Zhao, Y. Zhou, J. Chen, *Nat. Electron.* **2022**, *5*, 142.
[2] Y. Yang, W. Gao, *Chem. Soc. Rev.* **2019**, *48*, 1465.
[3] Y. Liu, X. Zhou, H. Yan, Z. Zhu, X. Shi, Y. Peng, L. Chen, P. Chen, H. Peng, *Adv. Funct. Mater.* **2022**, *32*, 2201510.
[4] D. Chen, Q. Pei, *Chem. Rev.* **2017**, *117*, 11239.
[5] X. Xu, S. Xie, Y. Zhang, H. Peng, *Angew. Chem., Int. Ed.* **2019**, *58*, 13643.
[6] X. Kang, Z. Zhu, T. Zhao, W. Zhai, J. Xu, Z. Lin, K. Zeng, B. Wang, X. Sun, P. Chen, H. Peng, *Adv. Funct. Mater.* **2022**, *32*, 2207763.
[7] W. J. Zhai, Z. F. Zhu, X. M. Sun, H. S. Peng, *Adv. Fiber Mater.* **2022**, *4*, 1293.
[8] R. Liu, Z. L. Wang, K. Fukuda, T. Someya, *Nat. Rev. Mater.* **2022**, *7*, 870.
[9] G. Chen, Y. Li, M. Bick, J. Chen, *Chem. Rev.* **2020**, *120*, 3668.
[10] B. E. Hardin, H. J. Snaith, M. D. McGehee, *Nat. Photonics* **2012**, *6*, 162.
[11] Y. Wang, M. I. Dar, L. K. Ono, T. Zhang, M. Kan, Y. Li, L. Zhang, X. Wang, Y. Yang, X. Gao, *Science* **2019**, *365*, 591.
[12] M. R. Lee, R. D. Eckert, K. Forberich, G. Dennler, C. J. Brabec, R. A. Gaudiana, *Science* **2009**, *324*, 232.
[13] M. Freitag, J. Teuscher, Y. Saygili, X. Zhang, F. Giordano, P. Liska, J. Hua, S. M. Zakeeruddin, J.-E. Moser, M. Grätzel, A. Hagfeldt, *Nat. Photonics* **2017**, *11*, 372.
[14] M. Mainville, M. Leclerc, *ACS Energy Lett.* **2020**, *5*, 1186.
[15] Y. Cui, Y. Wang, J. Bergqvist, H. Yao, Y. Xu, B. Gao, C. Yang, S. Zhang, O. Inganäs, F. Gao, J. Hou, *Nat. Energy* **2019**, *4*, 768.
[16] Y. Cao, Y. Liu, S. M. Zakeeruddin, A. Hagfeldt, M. Grätzel, *Joule* **2018**, *2*, 1108.
[17] Masud H. Z., H. K. Kim, *Mater. Today Energy* **2023**, *34*, 101299.
[18] M. Aftabuzzaman, S. Sarker, C. Lu, H. K. Kim, *J. Mater. Chem. A* **2021**, *9*, 24830.
[19] S. Pimputkar, J. S. Speck, S. P. DenBaars, S. Nakamura, *Nat. Photonics* **2009**, *3*, 180.
[20] W. Weng, P. Chen, S. He, X. Sun, H. Peng, *Angew. Chem., Int. Ed.* **2016**, *55*, 6140.
[21] X. Shi, Y. Zuo, P. Zhai, J. Shen, Y. Yang, Z. Gao, M. Liao, J. Wu, J. Wang, X. Xu, Q. Tong, B. Zhang, B. Wang, X. Sun, L. Zhang, Q. Pei, D. Jin, P. Chen, H. Peng, *Nature* **2021**, *591*, 240.
[22] J. He, C. Lu, H. Jiang, F. Han, X. Shi, J. Wu, L. Wang, T. Chen, J. Wang, Y. Zhang, H. Yang, G. Zhang, X. Sun, B. Wang, P. Chen, Y. Wang, Y. Xia, H. Peng, *Nature* **2021**, *597*, 57.
[23] M. Liao, C. Wang, Y. Hong, Y. Zhang, X. Cheng, H. Sun, X. Huang, L. Ye, J. Wu, X. Shi, X. Kang, X. Zhou, J. Wang, P. Li, X. Sun, P. Chen, B. Wang, Y. Wang, Y. Xia, Y. Cheng, H. Peng, *Nat. Nanotechnol.* **2022**, *17*, 372.
[24] L. Xie, W. Song, J. Ge, B. Tang, X. Zhang, T. Wu, Z. Ge, *Nano Energy* **2021**, *82*, 105770.
[25] R. Steim, T. Ameri, P. Schilinsky, C. Waldauf, G. Dennler, M. Scharber, C. J. Brabec, *Sol. Energy Mater. Sol. Cells* **2011**, *95*, 3256.
[26] L.-K. Ma, Y. Chen, P. C. Y. Chow, G. Zhang, J. Huang, C. Ma, J. Zhang, H. Yin, A. M. Hong Cheung, K. S. Wong, S. K. So, H. Yan, *Joule* **2020**, *4*, 1486.
[27] Y. M. Ren, D. Zhang, J. J. Suo, Y. M. Cao, F. T. Eickemeyer, N. Vlachopoulos, S. M. Zakeeruddin, A. Hagfeldt, M. Gratzel, *Nature* **2022**, *613*, 60.
[28] W. Duangthongsuk, S. Wongwises, *Exp. Therm. Fluid Sci.* **2009**, *33*, 706.

[29] L. Fedele, L. Colla, S. Bobbo, *Int. J. Refrig.* **2012**, *35*, 1359.
[30] H. D. Koca, S. Doganay, A. Turgut, I. H. Tavman, R. Saidur, I. M. Mahbubul, *Renewable Sustainable Energy Rev.* **2018**, *82*, 1664.
[31] J. Wu, Z. Lan, J. Lin, M. Huang, Y. Huang, L. Fan, G. Luo, Y. Lin, Y. Xie, Y. Wei, *Chem. Soc. Rev.* **2017**, *46*, 5975.
[32] H. Peng, M. Jain, Q. Li, D. E. Peterson, Y. Zhu, Q. Jia, *J. Am. Chem. Soc.* **2008**, *130*, 1130.
[33] Y. Bai, I. Mora-Sero, F. De Angelis, J. Bisquert, P. Wang, *Chem. Rev.* **2014**, *114*, 10095.
[34] Z.-S. Wang, H. Kawauchi, T. Kashima, H. Arakawa, *Coord. Chem. Rev.* **2004**, *248*, 1381.
[35] C.-Y. Chen, J.-H. Chang, K.-M. Chiang, H.-L. Lin, S.-Y. Hsiao, H.-W. Lin, *Adv. Funct. Mater.* **2015**, *25*, 7064.
[36] N. K. Elumalai, A. Uddin, *Energy Environ. Sci.* **2016**, *9*, 391.
[37] I. P. Liu, W. H. Lin, C. M. Tseng-Shan, Y. L. Lee, *ACS Appl. Mater. Interfaces* **2018**, *10*, 38900.
[38] J. Bisquert, *J. Phys. Chem. B* **2002**, *106*, 325.
[39] J. Bisquert, F. Fabregat-Santiago, I. Mora-Sero, G. Garcia-Belmonte, S. Gimenez, *J. Phys. Chem. C* **2009**, *113*, 17278.
[40] A. Zaban, M. Greenshtein, J. Bisquert, *ChemPhysChem* **2003**, *4*, 859.
[41] Z. Yang, H. Sun, T. Chen, L. Qiu, Y. Luo, H. Peng, *Angew. Chem., Int. Ed.* **2013**, *52*, 7545.

